PCCP

Influence of the polymer backbone rigidity on polyelectrolyte–surfactant complexes at the air/water interface†

Hernan Ritacco,‡ Pierre-Antoine Albouy, Amitabha Bhattacharyya and Dominique Langevin*

Laboratoire de Physique des Solides, Université Paris Sud, Bât 510, 91405 Orsay, France

Received 12th June 2000, Accepted 24th July 2000
First published as an Advance Article on the web 21th September 2000

We report dynamic surface tension and X-ray reflectivity studies on mixed polyelectrolyte–surfactant solutions. We have studied two different polyelectrolytes, polyacrylamide sulfonate, with a flexible backbone and xanthan, with a rigid backbone. We compare the results with the surface rheology and foaming behaviour of the same solutions. The static and dynamic properties of the mixed surface layers are similar for the solutions with the two polymers, only the behaviour upon large compressions is different. This might be at the origin of the differences in foamability and foam film stability observed with the two systems.

Introduction

The study of interactions between surfactants and polymers is now an important field of interest in colloid science.[1] Many practical systems for industrial applications contain mixtures of polymers and surfactants. These mixtures are used as thickeners in water-based formulations such as paints, drilling muds, *etc.* Of particular interest are the polyelectrolytes with rigid backbone such as xanthan, as their solutions in water possess interesting properties like large swelling ability and pronounced shear thinning effects. The interactions of xanthan with surfactants of opposite charge such as DTAB (dodecyltrimethylammonium bromide) have still received little attention. In a previous paper, we have studied the foams made with solutions of these two compounds.[2] These foams are very unstable and, contrary to foams made with pure surfactants, little relation was found with the surface rheological properties. In the present paper, we have investigated the role of the xanthan concentration on the surface complexes, and the adsorption kinetics. We have also studied the non-equilibrium behaviour upon compression. We will relate these new observations to the foam behaviour. For comparison purposes, we have performed similar studies with a flexible polyelectrolyte, polyacrylamide sulfonate (PAMPS), which will also be described.

Experimental

Materials

The cationic surfactant, dodecyltrimethylammonium bromide (DTAB) was obtained from Aldrich (99%) and was recrystallized (2 g of DTAB : 10 ml of ethyl acetate : 1 ml of ethyl alcohol) three times before use.

Xanthan is an extracellular polysaccharide produced by fermentation of the microorganism *Xanthomonas campestris.* Its primary structure, as shown in Fig. 1, consists of a linear 1–4 linked D-glucan chain substituted on every glucose residue by a trisaccharide side chain. The polymer has been obtained from International (now Dowell) Drilling Fluids (IDF) and thoroughly purified using microfiltration at low flow rate through decreasing sizes of micropore filters and ultrafiltration with a molecular cut-off of 20 000 Da.§ The weight-average molecular weight M_w of the sample, as measured by size exclusion chromatography (SEC) coupled with multiangle light scattering, is 1.8×10^6 g mol^{-1}.

PAMPS is an anionic statistical copolymer of neutral monomers of acrylamide and charged monomers of (acrylamidomethyl)propane sulfonate. A copolymer with a 10% number fraction of ionized monomers was used. The polymer was obtained from SNF Floerger, dissolved in deionized water (Millipore Milli-Q System) and purified with an ultrafiltration unit with a 20 000 cut-off membrane. The molecular weight M_w is 4.1×10^5 g mol^{-1}. We refer to this polymer as PAMPS 10%.

Xanthan has a rigid backbone, whereas PAMPS is more flexible, their intrinsic persistence lengths being respectively 50 Å (for xanthan in pure water)[3] and 10 Å.[4] In the presence of salt, xanthan takes a double helix configuration that is much more rigid, the persistence length being 1400 Å.[5] Single helix

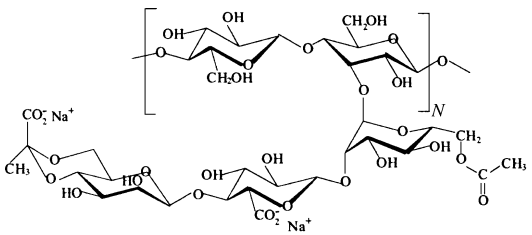

(a)

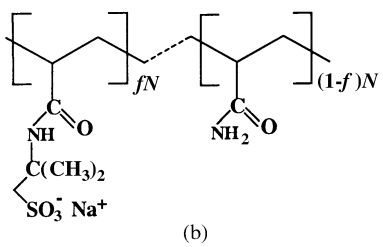

(b)

Fig. 1 Chemical structure of the polymers (a) xanthan and (b) PAMPS ($f = 0.1$).

† Presented at the Research Conference on Adsorption to Interfaces, Guildford, UK, April 12–14, 2000.

‡ Permanent address: Laboratorio de Sistemas Liquidos, Facultad de Ingenieria, 850 Paseo Colon, Buenos Aires, Argentina.

§ 1 Da (dalton) ≈ $1.660\,54 \times 10^{-27}$ kg.

configurations can also be obtained, with a persistence length of 400 Å.[3,5].

The structures of both polymers are shown in Fig. 1, and their characteristics in Table 1. The polymers were given to us by J. F. Argiller, Institut Français du Pétrole.

Methods

Surface tension. Surface tension measurements were carried out in a circular Teflon trough (capacity 5 ml) housed in a Plexiglass box. The surface tension was measured with an open-frame version of the Wilhelmy plate: The rectangular open-frame (20 mm × 10 mm), made of platinum wire, was attached to a force transducer mounted on a motor allowing it to be drawn away from the surface at a controlled constant rate. After pouring the solution into the trough, the surface tension was measured every 10 min until a constant value was reached (constant for 30 min). This allowed us to investigate the adsorption kinetics. The reproducibility (before precipitation) was ± 1 mN m^{-1} for the solutions with xanthan, a little better with PAMPS. The reproducibility with pure surfactant solutions was higher, ± 0.1 mN m^{-1}. In this case, the measurements were in agreement with literature data. The poorer reproducibility when the polymers are present is associated to long equilibration kinetics and probably to the difficulties to approach the final equilibrium state.[6] As we will see in the following, the mixed monolayers do not behave as equilibrium adsorbed layers.

X-ray reflectivity. Measurements were performed on a home-built set-up working in the angular dispersion mode.[7] This technique, first developed by Naudon *et al.*,[8] allows an easy and rapid record of reflection spectra. The q-range is limited to a maximum value of 0.35 Å^{-1} by the precision of the background correction. Specular reflection of X-ray provides information on the electron density in the direction normal to the liquid/air interface. For X-rays, the index of refraction (n) depends only on the electron density (ρ):

$$n = 1 - (r_0 \lambda^2/2\pi)\rho = 1 - \delta \quad (1)$$

where r_0 is the classical radius of the electron ($r_0 = 2.818 \times 10^{-15}$ m) and λ the X-ray wavelength ($\lambda = 1.542$ Å). In general, the index of refraction deviates by less than 10^{-5} from 1. The reflectivity can then be approximated by the Fresnel reflectivity (R_F) of an infinitely sharp interface modulated by interference effects from the thin surface layer.

$$\frac{R}{R_F} = \left| \frac{1}{\rho_{sub}} \int \rho'(z) \exp(iqz)\, dz \right|^2 \quad (2)$$

where ρ_{sub} is the electron density of the bulk phase, $\rho'(z)$ the gradient of the electron density along the surface normal and q the wave vector transfer normal to the surface. A convenient way to determine the electron density using eqn. (2) is to describe the film by a series of slabs of constant density whose parameters (electron density, ρ; the thickness, D and the roughness R) are then adjusted by a fitting procedure.[9] Here, we have modeled the absorbed layer by a single slab. Absorption corrections are not necessary with thin layers (thicknesses below 500 Å).

X-ray reflectivity experiments were carried out in a Teflon trough (~500 ml) with a Teflon barrier. This allowed us to compress the surface layers. The barrier can be moved forward in steps to increase the surface pressure. Let us recall that the surface pressure Π is the difference between the surface tension γ_0 of pure water and the surface tension γ measured in the presence of the adsorbed layer:

$$\Pi = \gamma_0 - \gamma \quad (3)$$

Surface viscoelasticity. The surface rheological properties have been investigated by using excited capillary waves. In this way, the surface compression elasticity and viscosity were measured in the frequency range $\omega = 100$–1000 Hz.[10]

The Gibbs elasticity is given by:

$$\varepsilon = A \frac{\partial \gamma}{\partial A} \quad (4)$$

where A is the surface area. This elasticity is the compression elasticity for an insoluble monolayer. When the surface is compressed, dissolution in the bulk or reorganisations in the surface layer can occur. This leads to dissipation and to a viscoelastic behavior conveniently described by a complex number:

$$\varepsilon(\omega) = \varepsilon_r(\omega) + i\varepsilon_i(\omega) = \varepsilon_r(\omega) + i\omega\kappa(\omega) \quad (5)$$

where ε_r is the compression elastic modulus, equal to the Gibbs elasticity ε at high frequency (when the monolayer does not have time to dissolve) and κ is the compression surface viscosity.[11]

The capillary wave system used is described in detail elsewhere.[10] The surface of the liquid was subjected to transverse (capillary) waves to determine the wavelength and decay coefficient of the waves. The viscoelastic coefficients were calculated using the dispersion equation and the value of the surface tension measured independently. These coefficients are not the pure compression coefficients, but the sum of the compression and shear coefficients. However, the shear coefficients are generally very small in soluble monolayers.[12]

Foam formation and stability studies. Foaming was studied using a vertical column consisting of a 50 cm long glass tube (diameter 3 cm) with a fritted glass filter at the bottom.[2] Nitrogen from a gas cylinder is blown through the filter and the solution located above. The flow rate was measured using a flow-meter. For a given gas flow rate, the height of the foam column in stationary conditions was taken as a measure of the foamability. To estimate the foam stability, we measured the time (T_r) taken by the foam to decay to half the original height after the gas flow was stopped. These results are qualitative in character and only allow a comparison of the foamability and foam stability of the different solutions.

Table 1 Properties of the polymers used in the present work[a]

	PAMPS	Xanthan
M_{poly}/g mol^{-1}	4.1×10^5	1.8×10^6
M_{mono}/g mol^{-1}	85	930
N	4800	2000
l_0[b]		
Simple helix/Å		400 ± 50[2,3]
Double helix/Å		1400 ± 200[3]
"Wormlike chain"/Å	10^4	50[2]
f	0.1	1.5
a/Å	2.5	10.3
A/Å	25	6.4[2]
v_{spe}/ml g^{-1}	0.77[29]	0.65[30]
δ[c]	4.70×10^{-6}	5.12×10^{-6}
ρ[c]/eÅ^{-3}	0.441	0.480

[a] Molar mass of the polymer M_{poly} and the monomer M_{mono}, degree of polymerization N, persistence length l_0, charge per monomer f, monomer size a, distance between consecutive charges A, specific volume v_{spe}, reduced electron density δ and electron density ρ. [b] The total persistence length l is the sum of the intrinsic one l_0, which is related to the molecular structure and the electrostatic one l_e, which describes the electrostatic repulsion between the charges along the chain. [c] $\rho = \delta \times (0.0938 \times 10^{36})$ $(\rho(H_2O) = (3.56 \times 10^{-6}) \times (0.0938 \times 10^{36}) = 0.334\ e$Å$^{-3})$ or $\rho = e_{mono} N_A / v_{spe} M_{mono}$.

Results

Surface tension

Our experiments were carried out with mixed solutions of surfactant and xanthan or PAMPS, with different concentrations.

The effect of the polymer concentration is shown in Figs. 2 and 3 for xanthan (concentrations 60, 175 and 357 ppm) and PAMPS (concentrations 57 and 116 ppm) respectively, as a function of surfactant concentration C_s. We see the usual synergistic lowering of surface tension γ at very low C_s in these systems. The surface tension is almost independent of the polymer concentration in this polymer concentration range. This is as observed earlier.[13–15] This fact can be explained by assuming that both surface complexation is an ion exchange process in which the surfactant and polymer counterions are expelled in the bulk and no polymer–surfactant complexes are formed in the bulk liquid.

We may recall that polystyrene sulfonate forms bulk aggregates at very small polymer and surfactant concentrations and does not behave in this way: large dependences of the surface tension with polymer concentration are observed with this polymer when mixed with DTAB.[15]

The curves for xanthan exhibit a short plateau beginning at 0.1 mM DTAB. Such plateaus are usually identified to the critical aggregation concentration (c.a.c.), that corresponds to the appearance of polymer–surfactant complexes in the bulk.[1] In the case of PAMPS 10%, no well-defined plateau is observed. Fig. 4 shows a comparison of the behaviour of the two polymers together with PAMPS 25%. When the polymer contains more ionized groups, the plateau is much more clearly visible. This was associated to the fact that the association in bulk is more cooperative for PAMPS 25% than for PAMPS 10%.[14] Xanthan is a strongly charged copolymer (average distance between two consecutive charges $A = 6.4$ Å), as compared with PAMPS 25% ($A = 10$ Å, see Table 1). Yet, its association co-operativity with DTAB is not as high as is

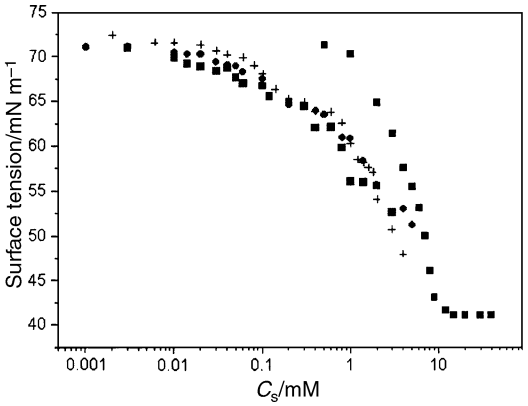

Fig. 2 Surface tension as a function of surfactant concentration C_s for 60 (crosses), 175 (circles) and 357 (squares) ppm xanthan. The surface tension of pure DTAB solutions is also shown for comparison (squares, largest tensions).

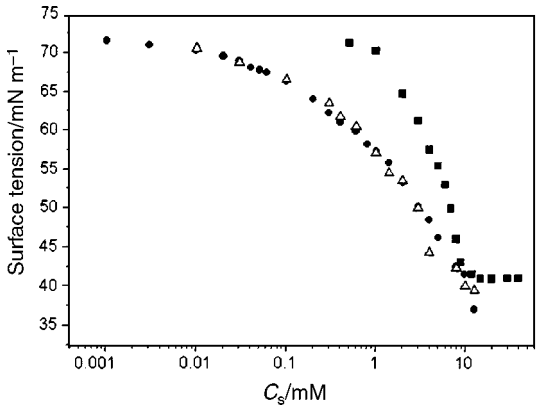

Fig. 3 Surface tension as a function of surfactant concentration C_s for 57 (triangles) and 116 (circles) ppm PAMPS 10%. The surface tension of pure DTAB solutions is also shown for comparison (squares).

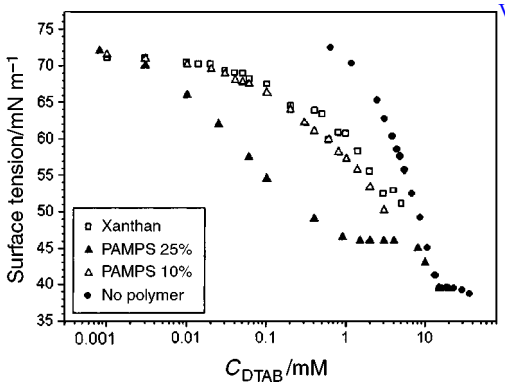

Fig. 4 Surface tension as a function of surfactant concentration C_s for xanthan and PAMPS 10 and 25%.

seen with PAMPS 25%, which has a flexible backbone. However, there are similarities in the surface tension curves for DTAB with xanthan or PAMPS 10%, indicating similarities in the surfactant–polymer affinities. So we decided to pursue the experiments with PAMPS 10%, to compare its behaviour with xanthan.

Typical dynamic surface tension curves (60 ppm xanthan and different DTAB concentrations) are shown in Fig. 5. When a fresh surface is created between the solution and air, the initial surface tension is that of the bare air/water interface. The surface tension begins to decrease only when the surface active species starts adsorbing at the interface. Different successive steps are involved in the equilibration process: motion towards the surface, transport through the subsurface (region affected by the vicinity of the surface, for instance by the surface electrostatic potential), reorganisation of the surface layer. In the case of simple surfactant solutions, when the bulk concentration is low and in the absence of convection, diffusion is expected to be the slowest step of the adsorption process. If one assumes that the characteristic times for the other processes are shorter, interfacial tension can be conveniently approximated by the following expression proposed by Serrien and Joos:[16]

$$\gamma = \gamma_{eq} + (\gamma_o - \gamma_{eq})\exp(-4k_d\, t/\pi)^{1/2} \qquad (6)$$

where γ, γ_{eq} and γ_o are the dynamic, equilibrium and pure solvent surface tensions respectively and k_d is the relaxation time constant. For a single adsorbing species, k_d is defined as:

$$k_d = D\left(\frac{dC}{d\Gamma}\right)^2 \qquad (7)$$

where D is the diffusion coefficient, Γ is the surface concentration and C is the bulk concentration. Eqn. (6) is valid when

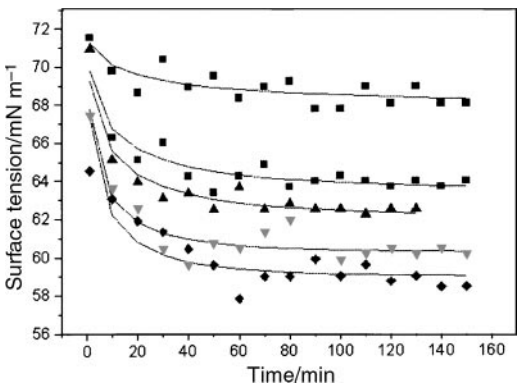

Fig. 5 Dynamic surface tension curves for 60 ppm xanthan and different C_s: from top to bottom C_s = 0.1, 0.4, 0.8, 1 and 1.4 mM.

$(\gamma_o - \gamma_{eq})$ is small (linearization allowed), *i.e.* at long enough times.

All the dynamic surface tension curves were fitted with this model, using $\gamma_o = 72.2$ mN m^{-1} (surface tension of pure water) to obtain k_d. In Fig. 6 we plot k_d as a function of C_s for different xanthan concentrations. All the curves show a surfactant concentration region with long relaxation times. For 60 ppm xanthan, this region coincides with the surface tension plateau (Fig. 2). For 175 and 357 ppm xanthan, long equilibrium times are observed even before the c.a.c. It should be noted that, depending upon xanthan concentration, precipitation can be noticeable in the concentration range of the plateau: for 357 ppm xanthan, precipitation begins above 0.4 mM DTAB, which corresponds well to the point where the amount of charges from the two species are equal (0.57 mM DTAB). For 60 and 175 ppm xanthan, precipitation could only be observed around 0.4 mM DTAB, although one would have expected to see it before. Perhaps the amount of precipitate is too small to be seen by the eye at lower DTAB concentrations.

The dependence of k_d on C_s for PAMPS is shown in Fig. 7. The dependence is qualitatively similar to xanthan. Here, precipitation occurs well after c.a.c., so the measurements could be made at higher surfactant concentrations. A second region of slow adsorption is observed above 1 mM DTAB.

X-ray reflectivity

X-ray reflectivity measurements have been carried out on mixed solutions of 60 ppm xanthan at different C_s. Fig. 8 shows the reflected intensity as a function of wave vector together with the fit for solutions of 60 ppm xanthan and 1 mM DTAB. All the curves are rather similar and most of the results will be presented in tables in the following.

We have checked independently with pure DTAB solutions that the surfactant contribution to the reflectivity is negligible,

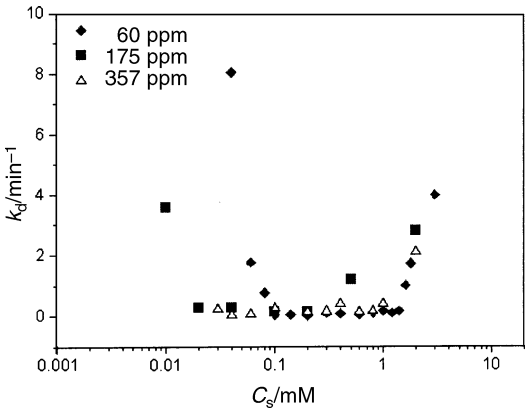

Fig. 6 k_d as a function of C_s, for 60, 175 and 357 ppm xanthan.

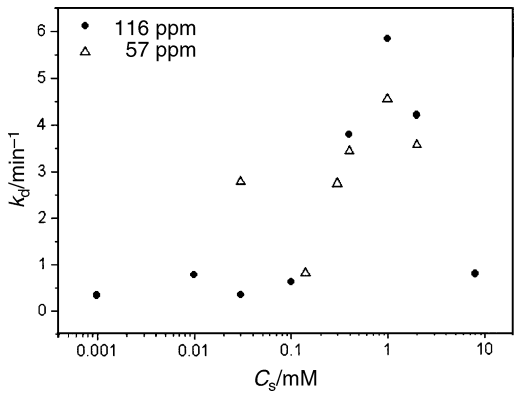

Fig. 7 k_d as a function of C_s, for 57 and 116 ppm PAMPS.

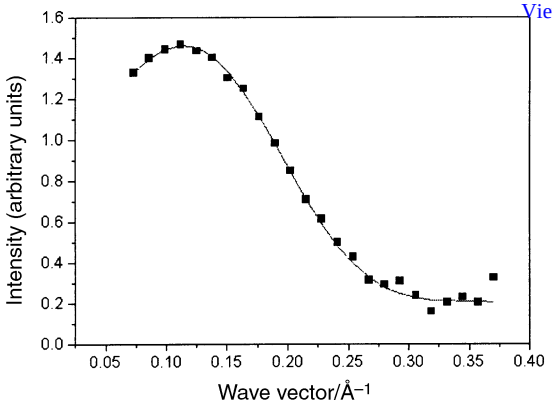

Fig. 8 X-ray reflected intensity as a function of wave vector for 60 ppm xanthan and 1 mM DTAB.

due to unfavourable contrast conditions.[17] Counterions being excluded from the surface region (see the surface tension paragraph above), the data reported in the tables correspond therefore to the polymer layers only.

The time variation of the interface thickness for $C_s = 0.005$, 0.05, 0.4 and 1 mM, corresponding to three different regions on the relaxation time curves has been investigated. There is no appreciable time dependence between 10 and 250 min, the time $t = 0$ corresponding to the time at which the solution was poured into the trough:

$C_s = 0.005$ mM	$h = (20.8 \pm 0.5)$ Å
$C_s = 0.05$ and 0.4 mM	$h = (19 \pm 1)$ Å
$C_s = 1$ mM	$h = (19.8 \pm 0.5)$ Å

the time variations being random. No appreciable variation with surfactant concentration is seen either.

These thicknesses are slightly smaller than those measured previously with larger xanthan concentrations (410 ppm): $h \sim (26 \pm 2)$ Å, for surfactant concentrations between 0.1 and 2 mM DTAB.[17] This might be due to the vicinity of the precipitation conditions, which might be responsible for a slight thickening of the mixed layers.

We have also checked the role of addition of salt. It is admitted that in the absence of added salt, the xanthan molecules are dissolved in water in the form of random coils. When enough salt is present, the chains associate in a double helix configuration, exactly as in the case of DNA.[5] We have compared xanthan solutions without and with salt added (4.6 mM KBr, conditions where double helices should be present). We did not see any significant differences in the reflectivity curves. These solutions have identical surface tensions within experimental errors. All this suggests that independent of the bulk chain configuration, the surface configurations of the xanthan chains are the same.

At this stage, we started compression experiments with 60 ppm xanthan solutions and various DTAB concentrations: 0.05, 0.52 and 1 mM. Fig. 9 shows the surface pressure variation with surface layer area for $C_s = 1$ mM. The curve shows an inflexion point, that could indicate a phase transition in the mixed layer. Similar features are observed at the other DTAB concentrations: pseudoplateaus around 26 mN m^{-1}, maximum pressures above 30 mN m^{-1}. Fig. 10 shows the evolution of the reflectivity curves as the layer is compressed: a clear thickness increase is observed. Above the pseudoplateau, the quality of the fits deteriorates (especially at low q), indicating that the approximation of layer homogeneity (one slab model) is probably no longer appropriate. When the layers are compressed after adsorption equilibrium has been attained, the new equilibrium is reached very fast. Furthermore, the behaviour upon compression is fully reversible: when a layer is fully decompressed after compression to pres-

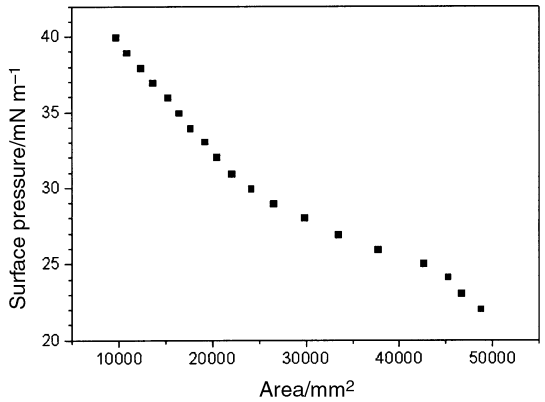

Fig. 9 Surface pressure as a function of surface area for 60 ppm xanthan and 1 mM DTAB.

sures around 35 mN m^{-1}, the fits of the reflectivity curves lead to parameters identical to those obtained before compression. The complete data from the fits are reported in Table 2.

The characteristics of the mixed layers with PAMPS are similar. The main difference is the roughness of the layer/solution interface, which is larger for the PAMPS layers. For $C_s = 15$ mM, the thickness jumps to a value around twice the value at low surfactant concentrations, this effect being reproducible. This is associated with the onset of precipitation in the bulk. A thickening of the layer was also observed by ellipsometry in the precipitation region.[14] The parameters from the fits are given in Table 3.

The behaviour of mixed DTAB–PAMPS 10% layers on compression is very different from DTAB–xanthan layers. The surface layer cannot be compressed to a state where the surface pressure is large, larger than the maximum surface pressure at equilibrium: the layers adsorbed from the most concentrated solutions cannot be compressed at all. Furthermore, surface pressures larger than equilibrium surface pressures can only be reached upon rapid compression: stable and reversible surface pressure curves such as those of Fig. 9 for xanthan cannot be obtained. During the pressure increase, the thickness increases and the roughness of the layer/solution interface decreases, except for $C_s = 15$ mM, for which the thickness falls to a lower value (Table 3).

Table 2 Parameters for the X-ray reflectivity fits. Solutions of 60 ppm xanthan, for different surfactant concentrations and different surface pressures Π[a]

C_s/mM	Π/mN m^{-1}	$\delta/10^{-6}$	R_{am}/Å	R_{mw}/Å	D/Å
0.05	9	4.09	3.9	3.5	21.3
	12	4.16	4.2	3.7	21
	15	4.23	4.4	4.3	22.4
	18	4.22	4.3	3.4	23.6
	21	4.23	4.5	3.5	24.4
	34	4.23	5	1	30
0.52	24 (before compression)	4.20	3.9	3.0	21.9
	26	4.65	Poor fit		23.8
	26	4.95	Poor fit		25.2
	28	4.4	Poor fit		28.2
	32	4.6	Poor fit		31
	35	4.63	Poor fit		29.8
	24 (after compression)	4.17	3.8	2.8	21.5
1	22	4.21	4.4	3.1	23.7
	24	4.19	4.6	3.2	24.9
	26	4.15	4.6	3.4	26.3
	28	4.09	4.6	2.1	27.1
	30	4.11	4.7	2	27
	32	4.38	Poor fit		29.3
	34	4.23	Poor fit		30.9
	36	4.16	Poor fit		31.4
	38	4.33	Poor fit		31.9
	40	4.25	Poor fit		33.7

[a] δ, reduced electron density, R_{am}, roughness of the air/layer interface, R_{mw}, roughness of the layer/solution interface, D, layer thickness.

Surface viscoelasticity

The results of the viscoelasticity measurements are described in detail elsewhere.[2] At low C_s, the values of the real and

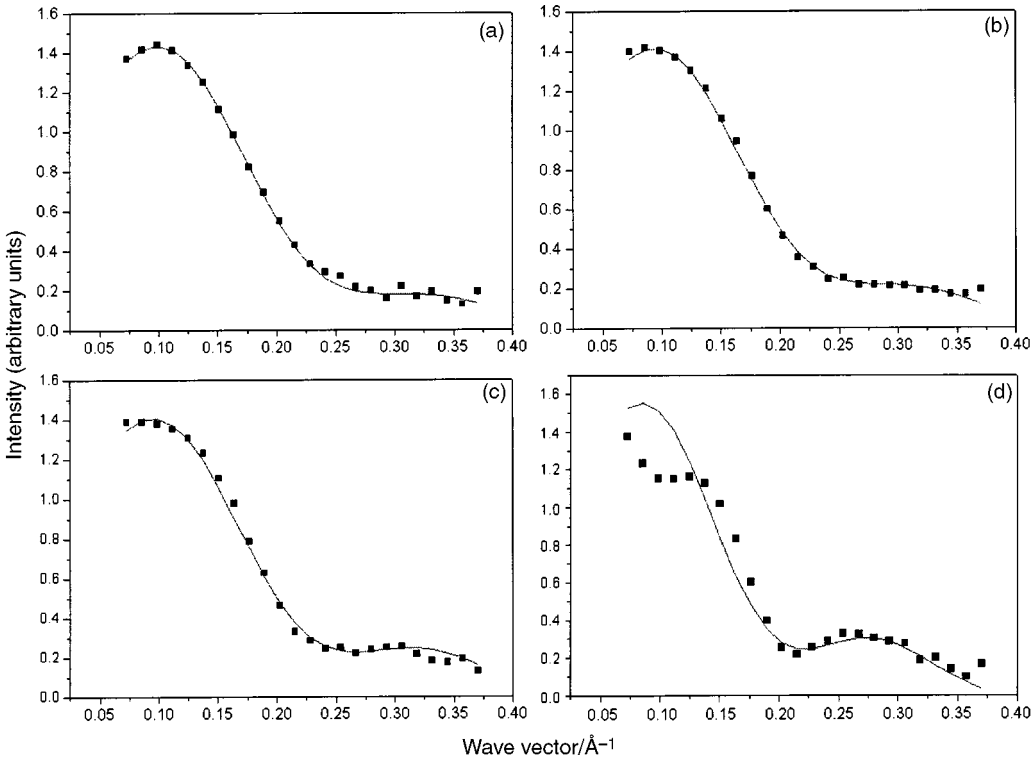

Fig. 10 X-ray reflected intensity as a function of wave vector for 60 ppm xanthan and 1 mM DTAB solutions after compression of the surface layers: (a) $\Pi = 24$ mN m^{-1}, (b) $\Pi = 26$ mN m^{-1}, (c) $\Pi = 29$ mN m^{-1}, (d) $\Pi = 34$ mN m^{-1}.

Table 3 Parameters for the X-ray reflectivity fits. Solutions of 116 ppm PAMPS 10%, for different surfactant concentrations and different surface pressures Π[a]

C_s/mM	Π/mN m^{-1}	$\delta/10^{-6}$	R_{am}/Å	R_{mw}/Å	D/Å
0.1		4	3.8	11.7	20
0.5	14.7 (compressed)	4.08	4.4	6.3	22
	18	3.88	4	7	28
	22	3.97	4.6	4	26
	26	3.92	4.9	3	29.1
1.2	12	3.94	3.9	7	25.4
2	15	4.12	3.9	12	22
5	18	4	4	8	24.6
	28.8 (compressed)	3.8	4	5	26
	30	3.79	4.1	4	27.6
	32	3.71	4.3	3	29
10	21	3.9	4	5.9	26.5
15	34		3.5	5.4	43
	36.5 (compressed)	3.74	3.7	6	25

[a] δ, reduced electron density, R_{am}, roughness of the air/layer interface, R_{mw}, roughness of the layer/solution interface, D, layer thickness.

imaginary parts of the viscoelastic moduli are small, and sometimes ε_i is negative (Fig. 11). As C_s is increased, the values of the two coefficients increase, reach a maximum and then decrease again.

Foam formation and stability

The results from the foaming studies are shown in Fig. 12. There is almost no foaming for C_s less than 0.01 mM. For xanthan, there is an increase in the foam height upon increasing C_s beyond 0.06 mM. The height increases with C_s up to 0.3 mM, decreases after and then increases again very fast. For PAMPS, there is an increase in foam height above 0.06 mM DTAB. The increase here is much larger than in the case of xanthan. This is followed by a slight decrease at around 0.5

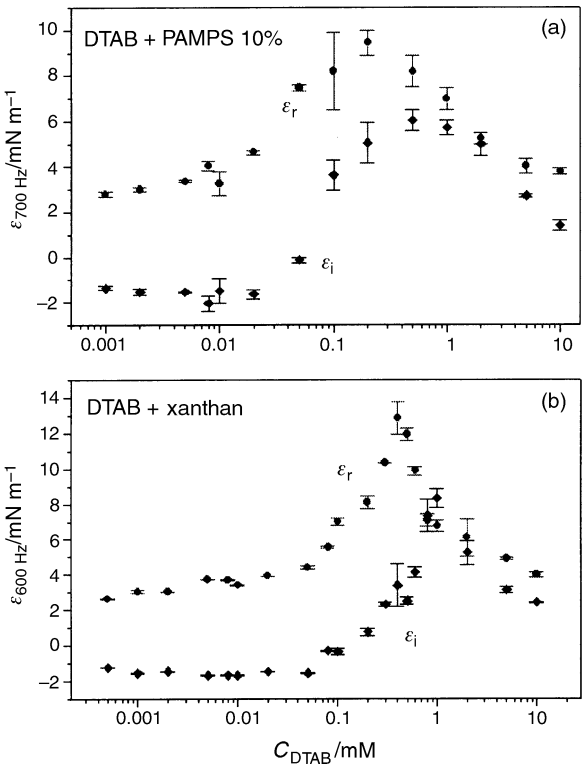

Fig. 11 Surface viscoelasticity as a function of C_s for DTAB solutions with (a) PAMPS 10% and (b) xanthan.

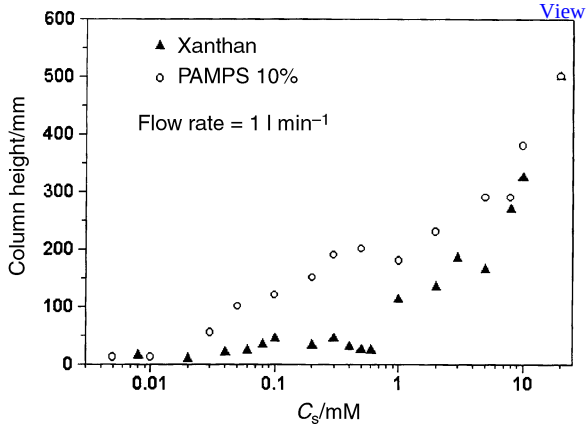

Fig. 12 Foam height as a function of surfactant concentration for the two solutions, at a constant flow rate of 1 l min^{-1} of nitrogen.

mM, though it is not as clear as in the case of xanthan. After this, there is a rapid increase in the foam height. It is interesting to note that the final increase in the foam height is almost independent of the polymer used. The values are almost identical for 20 mM surfactant for all solutions.

The foam stability results are shown in Fig. 13. The time of decay to half height (T_r) is very small for C_s less than 1 mM. After that, T_r increases slowly for xanthan. The increase becomes fast above 5 mM. In the case of PAMPS, the increase occurs above 5 mM, and is very abrupt. The behaviour of the two solutions becomes similar after 5 mM.

Discussion

Surface tension

As it can be seen from the surface tension results, there is a synergistic lowering of γ for the mixed solutions for very small values of C_s. This indicates a complex formation between DTAB and the polymer at the surface, which attracts more surfactant to the surface and hence reduces γ. As C_s is increased, γ decreases till the c.a.c. is reached where there is a plateau. At this point, there is a formation of complexes between the polymer and the surfactant in bulk. The surface tension begins to decrease only after the complexation is complete and more surfactants can come to the surface. The length of the plateau depends upon the degree of cooperativity of the bulk complexation process. In the case of xanthan and PAMPS 10%, this cooperativity is not very marked: the plateau is not very flat for xanthan and is hardly visible for PAMPS 10%. The surface tension remains smaller than that

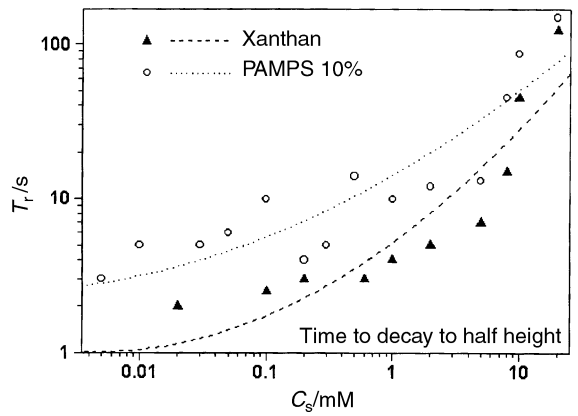

Fig. 13 Foam lifetimes T_r *vs.* surfactant concentration for the solutions. T_r is the time taken by the foam column to drop to half its original height after the gas flow is stopped. The lines are second order polynomial fits to the experimental points and are a guide to the eye.

of the pure surfactant, even close to the critical micellar concentration (c.m.c.). This indicates that the polymers are still present in the surface layers.[18]

The adsorption kinetics is considerably slowed down in the c.a.c. region. This is as observed qualitatively earlier, including for PAMPS 25%, for which the c.a.c. is better defined.[14] The effect is counterintuitive, since one could expect from relations of the type of eqn. (7) that the adsorption should become faster when bulk concentrations are increased. Application of eqn. (7) for surfactant alone leads to unrealistically large diffusion constants, in the range 10^{-9}–10^{-12} cm^2 s^{-1}. Rather, the competition between aggregation in bulk and at the surface might be responsible for this slowing down effect, as in the adsorption kinetics in micellar solutions:[19] the diffusion coefficient of the bulk aggregates is expected to be much larger than that of the single polymer chains. Furthermore, the time to exchange between the bulk and surface aggregates is probably extremely long. The adsorption kinetics becomes faster at the end of the c.a.c. plateau, this being associated with a vertical segregation in the mixed layer: as one approaches the c.m.c. of the pure surfactant solutions, the surfactant layer becomes denser, the polymers segments are all expelled below the surfactant monolayer, and the surface tension approaches that of the pure surfactant solution.[18,20,21] After the c.a.c. plateau, there are surfactant monomers in excess; their mobility being high, this could explain why the adsorption kinetics, as deduced from dynamic surface tension measurements, is accelerated.

The second slowing down region for PAMPS 10% is harder to explain. It might be associated with the vicinity of the precipitation, where microgels start to nucleate close to the surface and might reduce the local surfactant mobility.[14]

X-ray reflectivity

The X-ray reflectivity results give us the thickness of the polymer layers. Indeed, the contrast conditions are such that the pure surfactant monolayers are not detected, even around the c.m.c. In the case of xanthan, the thickness measured for layers obtained after adsorption from solutions is remarkably constant, and independent of various parameters: time, surfactant concentration, salt. The equilibrium thickness is reached well before the surface tension: for instance, for 0.4 mM DTAB–60 ppm xanthan solutions, it takes more than one hour to reach the equilibrium surface tension (Fig. 5), whereas the reflectivity curve does not change after 10 min. The long time part of the kinetics observed in dynamic surface tension in this case is associated to reorganisations in the surface layer which do not affect the thickness and the local density. The measured thickness is comparable to the radius of the xanthan in its double helix configuration.[5] The absence of influence of salt suggests that the adsorbed xanthan chains have a double helical configuration whatever be the bulk conformation. This might be due to the high local ionic concentration in the surface region.

The compressed monolayers are thicker, the thickness increasing with surface pressure. This fact is understandable if one assumes that once adsorbed, the chains cannot desorb back into the solution. Indeed, the energy gained during the adsorption process from the ion exchange is of the order of $fNkT$, where fN is the number of ionic groups in the polymer chain, k the Boltzmann constant and T the absolute temperature. This energy is therefore very large and prevents the surface complex from further dissociation.[6] It is however remarkable to see that the mixed layer behaves as an equilibrium insoluble monolayer: compression is followed quickly and is fully reversible. The nature of the 2D phase transition observed in Fig. 9 remains to be elucidated.

PAMPS 10% behaves in a very different way. It leads to less compressible layers, those for large DTAB concentrations being not compressible at all, and the compressed layers are less stable. This suggests that exchanges with the bulk are easier than in the case of xanthan. The roughness of the layer/solution interface is also larger than for xanthan. This might be due to the presence of loops, due to the polymer backbone flexibility and to the large distance between charges.[14] However, since the refractive index of the layer is close to that of water (similar δ), the accuracy on R_{mw}, the roughness of the layer/solution interface, is limited, and its variations can only indicate trends. When the layer is compressed, this roughness has a tendency to decrease. The decrease in thickness upon compression for $C_s = 15$ mM can be due to the expulsion of excess polymer attached to the surface above the precipitation conditions.

Surface rheology

For pure DTAB, the dependence of surface viscoelastic coefficients on the surfactant concentration can be explained by the Lucassen van den Tempel (LT) model,[10,22] According to this model, surfactant molecules dissolve into the underlying water on compression to restore the equilibrium surface concentration. When the monolayer is expanded, more surfactant molecules are adsorbed to the surface. Two extreme cases are easy to understand: when the frequency of the sinusoidal compression is low, the monolayer is always in equilibrium, hence: $\varepsilon_r = \varepsilon_i = 0$. When the frequency is high, the monolayer behaves like an insoluble monolayer, so: $\varepsilon_i = 0$ and ε_r is equal to the Gibbs elasticity (eqn. (3)). In the case of mixed layers, with free exchanges between surface and bulk, and no bulk aggregates present, the following expressions have been proposed for ε_r and ε_i[23]

$$\varepsilon_r = \varepsilon_s \frac{1+\Omega_s}{1+2\Omega_s+2\Omega_s^2} + \varepsilon_p \frac{1+\Omega_p}{1+2\Omega_p+2\Omega_p^2} \quad (8)$$

$$\varepsilon_i = \omega\kappa = \varepsilon_s \frac{\Omega_s}{1+2\Omega_s+2\Omega_s^2} + \varepsilon_p \frac{\Omega_p}{1+2\Omega_p+2\Omega_p^2} \quad (9)$$

with

$$\varepsilon_j = -\Gamma_j \frac{\partial\gamma}{\partial\Gamma_j} \quad \text{and} \quad \Omega_j = \sqrt{\frac{D_j}{2\omega}} \frac{\partial c_j}{\partial\Gamma_j}$$

It is not clear whether these expressions are applicable to the present case. The surface complex seems rather insoluble, so one would rather expect that $\varepsilon_r = \varepsilon_s + \varepsilon_p$ and $\varepsilon_i = 0$ if no intralayer relaxations are operating.

Following these lines, we have attempted to correlate the surface tension results to the surface viscoelasticity results. We have calculated the surfactant contribution first, by using the Gibbs equation applicable to this problem (ion exchange and no bulk aggregates approximation) to derive the surfactant surface concentration:[14]

$$\Gamma_s = \frac{1}{kT} \frac{\partial\gamma}{\partial \ln C_s} \quad (10)$$

By using the accepted value of the diffusion coefficient of DTAB (4×10^{-6} cm^2 s^{-1}), we have found that before c.a.c. $\varepsilon_s(\omega)$ is equal to the corresponding Gibbs elasticity ε_s. The results for xanthan are shown in Fig. 14a. Let us recall that the model is applicable only up to the c.a.c., as bulk aggregates appear after that, so the fit is limited to smaller concentrations. As can be seen, there is a good agreement between the experimental and calculated values of ε_r up to 0.1 mM DTAB, provided that a constant contribution of 2.5 mN m^{-1} is added to ε_s. This difference is likely to be the polymer contribution $\varepsilon_p = 2.5$ mN m^{-1}. The results are similar for PAMPS, including the ε_p value (Fig. 14b). In the region of validity of this treatment, the values of ε_i are negative instead

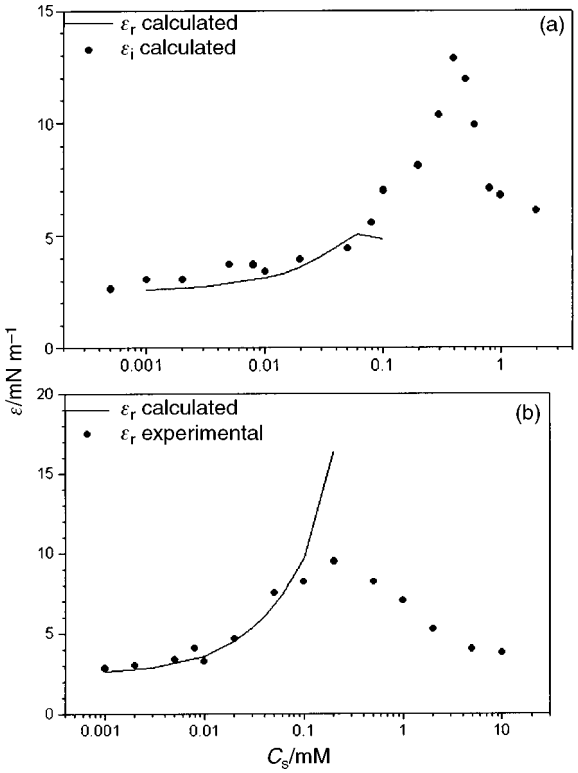

Fig. 14 Comparison of calculated and experimental values of the viscoelastic coefficients for solutions with (a) xanthan, (b) PAMPS.

of being zero. This feature is sometimes observed, but not understood at the moment.[24]

At higher surfactant concentrations, aggregates are probably formed in the bulk, and this treatment is no longer valid. It is interesting to note that the peak in elasticity occurs when k_d starts to increase for both polymers, *i.e.*, when the adsorption becomes faster. This could be due to the enhanced surfactant mobility, as suggested in the previous discussion.

It is somewhat surprising to see that the different dynamic behaviour of the surface complexes upon compression does not seem to be reflected in the viscoelastic behavior, very similar for the two polymers.

Foam formation and stability

Foam properties of solutions are generally related to the stability of the films separating the air bubbles. Good foamability demands that the bubble surfaces be rapidly covered by surfactant. In general, therefore, large foamabilities are well correlated to fast adsorption kinetics. Surprisingly here, the local foamability maximum around 0.1 mM DTAB occurs when the adsorption rate is minimum: see Figs. 6, 7 and 11. At larger surfactant concentrations, there is a better correlation between fast adsorption (Fig. 7) and good foamability. This is probably associated to the fact that at these concentrations, the surface pressure is essentially created by the surfactant and that even if the polymer–surfactant complexes have not enough time to be formed at the surface, the surfactant monolayer alone confers a good stability to the foam. Indeed good foamability also demands that the foam bubbles do not break too quickly. Foamability and foam stability are therefore closely related. Foam stability is governed by the following processes: (a) Drainage: removal of liquid from the space between the bubbles, and thinning of the films. The drainage rate is slightly less for more viscoelastic layers.[25] (b) Diffusion of gas from the small bubbles towards larger ones (Ostwald ripening), leading to a bubble size growth. Gas diffusion rate decreases with surface coverage.[26] (c) Coalescence: breaking of the film between adjacent bubbles to form one large bubble. A finite elasticity protects the films from rupture.[27]

All the phenomena depend on the elasticity and viscosity of the surface, and high elasticities and viscosities are thus expected to stabilize the foam. However, all the above processes occur at different timescales τ and the surface rheological parameters to be considered are those at a frequency $\omega = 1/\tau$.

As can be seen clearly for xanthan, the foam height begins to increase on reaching the value of C_s where surface viscosity becomes positive. This is also true for PAMPS. Although the surface rheological behaviour of the different polymers is similar, the foaming capacity is much larger with PAMPS than with xanthan. This could be related to the difference in surface layer behaviour upon compression: the solutions with xanthan give rise to insoluble types of layers, whereas the solutions with PAMPS give rise to layers potentially able to exchange material with the bulk solutions. Indeed, it is known that solutions of substances that give rise to insoluble surface layers (such as dodecanol for instance) do not foam, even when the surface layers have large compression elasticities (above 80 mN m^{-1} for dodecanol).[28]

The decrease in the foam height after the initial increase corresponds to the peak in ε_r. This is somewhat counterintuitive, since one would rather expect a coincidence between the peak in ε_r and the peak in foam height. It should be recalled however that the position of the peak in ε_r depends on the frequency ω: the larger the frequency, the larger is C_s at the peak. The characteristic frequency of the foaming phenomenon is much less than the frequencies investigated with the capillary waves device, and the intermediate foaming capacity maximum might possibly be related to the maximum in surface elasticity. After the local minimum in foam height, the foaming and foam stability of the solutions is larger. For 20 mM surfactant, there is hardly any difference between the two solutions and those of pure DTAB. This could mean that at this concentration the surfactant monolayer is compact and there is no more penetration of the polymer in the surface layer.

The foam stability behaviour of the polymers is also different. The intermediate maximum observed in the foam height variation with surfactant concentration is not present in the foam lifetime variation. Again the solutions with PAMPS 10% lead to more stable foams than the solutions with xanthan, the difference vanishing close to the c.m.c. of the surfactant.

Conclusion

To summarize, it is not straightforward to compare the foaming behaviour and the surface layers properties in these mixed polyelectrolyte–surfactant systems.

The surface tension is essentially independent of polymer concentration, in agreement with the ion-exchange model. The adsorption kinetics is slow in a surfactant concentration range around c.a.c., and becomes fast again close to the c.m.c. of the pure surfactant, where the surface layers with and without polymer become similar. When subjected to small compression–expansion cycles, the layers exhibit a viscoelastic response, similar for the two polymers. Below c.a.c., they behave as incompressible layers, with an elastic contribution of the polymer of about 2.5 mN m^{-1}, similar for the two polymers. Appreciable differences are seen only when the compression is more important (decrease of the surface area by a factor up to 5): the layers with xanthan still behave as insoluble layers (even above c.a.c.), whereas those with PAMPS are partially soluble. This particular difference might be associated to the large differences in foamability of the two polymers at small surfactant concentrations. It could also be related to the striking difference in foam film stability: PAMPS stabil-

izes DTAB foam films whereas it is impossible to form foam films in the presence of xanthan.[17]

Acknowledgements

We thank Institut Français du Pétrole and Ministère de la Recherche for financial support (H.R., program ECOS, project A98E04 and A.B, post-doctoral fellowship).

References

1 E. D. Goddard and K. P. Ananthapadmanabhan, *Interactions of Surfactants with Polymers and Proteins*, CRC Press, Boca Raton, FL, 1993.
2 A. Bhattacharyya, F. Monroy, J. F. Argillier and D. Langevin, *Langmuir*, in press.
3 M. Milas, M. Rinaudo, R. Duplessix, R. Borsali and P. Lindner, *Macromolecules*, 1995, **28**, 3119.
4 J. F. Argillier, Thèse de l'Université Paris VI, Paris, 1989.
5 L. Chazeau, M. Milas and M. Rinaudo, *Int. J. Polym. Anal. Charact*., 1995, **2**, 21.
6 M. Cohen Stuart and J. M. Kleijn, in *Physical Chemistry of Polyelectrolytes*, ed. Ts. Radeva, Marcel Dekker, New York, 2000.
7 P. A. Albouy and P Valerio, *Supramol. Sci*., 1997, **4**, 191.
8 A. Naudon, J. Chihab, P. Goudeau and J. Minmault, *J. Appl. Crystallogr*., 1989, **22**, 460.
9 R. M. Richardson and S. J. Roser, *Liq. Cryst*., 1987, **2**, 797.
10 C. Stenvot and D. Langevin, *Langmuir*, 1988, **4**, 1179.
11 D. Langevin, in *Light Scattering by Liquid Surfaces and Complementary Techniques*, ed. D. Langevin, Surfactant Science Series, Marcel Dekker, New York, 1992, vol. 41, ch. 11.
12 H. C. Maru and D. T. Wasan, *Chem. Eng. Sci*., 1979, **34**, 1295.
13 J. H. Buckingham, J. Lucassen and F. Hollway, *J. Colloid Interface Sci*., 1978, **67**, 423.
14 (*a*) A. Asnacios, D. Langevin and J. F. Argillier, *Macromolecules*, 1996, **29**, 7412; (*b*) A. Asnacios, D. Langevin and J. F. Argillier, *Eur. Phys. J. B*, 1998, **5**, 905.
15 R. v. Klitzing, A. Asnacios and D. Langevin, *Colloids Surf. A*, 2000, **167**, 189.
16 G. Serrien and P. Joos, *J. Colloid Interface Sci*., 1990, **139**, 149.
17 C. Stubenrauch, P. A. Albouy, R. v. Klitzing and D. Langevin, *Langmuir*, 2000, **16**, 3206.
18 B. Jean, L. T. Lee and B. Cabane, *Langmuir*, 1999, **15**, 7585.
19 J. Lucassen, *Faraday Discuss., Chem. Soc*., 1975, **59**, 76.
20 (*a*) A. Creeth, E. Staples, L. Thompson, I. Tucker and J. Penfold, *J. Chem. Soc., Faraday Trans*., 1996, **92**, 589; (*b*) D. J. Cooke, J. A. K. Blondel, J. R. Lu, R. K. Thomas, Y. Wang, B. Han, H. Yan and J. Penfold, *Langmuir*, 1998, **14**, 1990; (*c*) D. J. Cooke, C. C. Dong, J. R. Lu, R. K. Thomas, E. A. Simister and J. Penfold, *J. Phys. Chem. B*, 1998, **102**, 4912.
21 C. Stubenrauch, R. v. Klitzing, A. Asnacios, J. F. Argillier and D. Langevin, unpublished data.
22 (*a*) J. Lucassen and M. van den Tempel, *Chem. Eng. Sci*., 1972, **271**, 1283; (*b*) J. Lucassen and M. van den Tempel, *J. Colloid Interface Sci*., 1972, **41**, 491.
23 R. Miller and K. Kretzschmar, *Adv. Colloid Interface Sci*., 1991, **37**, 91.
24 F. Monroy, J. Kahn and D. Langevin, *Colloids Surf. A*, 1998, **143**, 251.
25 M. Durand, G. Martinoty and D. Langevin, *Phys. Rev. E*, 1999, **60**, R6307.
26 S. Cohen-Addad and D. Quéré, in *Soft Order in Physical Systems*, Plenum, New York, 1994.
27 D. Langevin, *Curr. Opin. Colloid Interface Sci*., 1998, **3**, 600.
28 H. Fruhner, K. D. Wantke and K. Luckenheimer, *Colloids Surf. A*, 2000, **162**, 193.
29 F. Millet, M. Nedyalkov, B. Renard, F. Lafuma and J. Benattar, *Langmuir*, 1995, **15**, 2112.
30 M. Rinaudo, personal communication.